

Short Communication

Corrosion Behaviour of TiN and CrN Coatings Produced by Magnetron Sputtering Process on Aluminium Alloy

Xiaona Suo¹, Chun Guo¹, Decheng Kong^{2*}, Li Wang²

¹No.704 Research Institute of China Shipbuilding Industry Corporation, Shanghai 200031, China

²Institute for Advanced Materials and Technology, University of Science and Technology Beijing, Beijing 100083, China

*E-mail: 15201461811@163.com

Received: 7 June 2018 / Accepted: 16 October 2018 / Published: 30 November 2018

In this study, the corrosion properties of TiN and CrN coatings on aluminium alloy fabricated by magnetron sputtering were studied by using electrochemical techniques such as potentiodynamic measurement and salt spray tests. Results showed that CrN coatings exhibited a better corrosion resistance on aluminium alloy when compared to TiN coatings with the same thickness. The inferior corrosion performance of TiN coating is not a result of the intrinsic corrosion behaviour of the nitride coating itself but is a result of small structural defects, e.g., pinholes and cracks formed during deposition, which act as channels for the corrosion of the substrate.

Keywords: Aluminum alloy; TiN; ZrN; Magnetron sputtering; Corrosion

1. INTRODUCTION

7000-series aluminium alloys are widely used in the manufacturing industry of advanced equipment, such as spacecraft structures and high-speed-train car bodies, owing to their excellent mechanical properties, including high specific stiffness and high specific strength [1]. Advanced equipments have rigidity requirements for long-term safety and reliability throughout their life cycle. However, the performance of 7000-series aluminium alloys in industrial and marine atmosphere environments is not satisfactory owing to their high inherent susceptibility to corrosion. Corrosion often occurs on aluminium alloys and usually involves the adsorption of ions on a surface, reaction of the anion (e.g. Cl⁻) with aluminium in the surface oxide layer, thinning of the oxide layer by reaction/dissolution, and direct attack of the exposed substrate [2]. Corrosion has caused an annual financial loss of US\$4 trillion globally, half of which is due to the corrosion damages and the other is attributed to the investment of corrosion protection [3], and more and more researchers now have paid

effects on the development of corrosion-resistant materials [4-7]. Passivity is the key for many materials that against corrosion, such as stain steel, aluminium-based alloys and copper-based alloys [8-13], and the passive film on metals has been verified to be composed of a compact barrier layer and an outer precipitated layer. However, many inclusions exist in the aluminium alloy, compromising the corrosion resistance greatly, especially for pitting corrosion resistance. As in this case, surface treatment must be taken into consideration and surface coating is an effective way to protect the matrix against corrosion, numerous studies have been conducted on this topic [14-21]. Non-metallic coating materials such as TiN or CrN coating were found to be satisfied by the formation of bonds with other reactive ions and they are chemically unreactive [22, 23]. The corrosion resistance of TiN coating prepared by physical vapor deposition (PVD) is mainly controlled by the amount of open porosity in the TiN layer and the columnar structure and defects formed during the PVD process such as voids, pinholes, pores, cracks and even delamination could lead to open paths between the substrate and the corrosive environment, as well as for ZrN coating [24]. Magnetron sputtering has developed rapidly over the past few decades and magnetron sputtered coatings now outperform coatings deposited by other PVD processes, and can offer the similar functionality as much thicker coatings produced by other surface coating techniques [25]. However, there were not many direct results about the anti-corrosion property comparing those two coatings prepared by magnetron sputtering with the same thickness.

In this study, the TiN and CrN coatings were produced on the aluminium alloy by magnetron sputtering with the same thickness (around 2 μm), respectively, and the top-surface and cross-sectional morphologies were observed by scanning electron microscopy (SEM). The element content and distribution were obtained by energy-dispersive spectroscopy (EDS). Electrochemical techniques such as potentiodynamic measurement and salt spray tests were conducted to compare the corrosion behaviour of these two coatings. The findings are expected to contribute valuable information for developing coating methods on aluminium alloys for future applications.

2. EXPERIMENTAL METHODS

2.1. Materials preparation

Aluminium alloy foils (known as 7B05-T5 in engineering materials), whose compositions include Si of 0.065 wt. %, Fe of 0.18 wt. %, Cr of 0.23 wt. %, Cu of 0.16 wt. %, Mn of 0.37 wt. %, Zn of 4.38 wt. %, Mg of 1.04 wt. %, and the remaining element Al, with a size of 20 mm \times 20 mm \times 2.5 mm were used as substrates.

The coatings were deposited using a CFUBMSIP system (Teer Coatings, Ltd.). Before TiN or CrN deposition, the aluminium alloy was first sputtered by Ar ions bombardment at a bias voltage of –500 V to remove the oxide films formed in the air. Then, a Ti or Cr coating as an interlayer was deposited for 600 s to improve adhesion and to reduce stress at the substrate interface. Finally, the TiN or CrN coating was deposited by sputtering a pure metal titanium (99.9%) or chromium (99.9%) target in a gas mixture atmosphere of Ar (99.99%) and N₂ (99.99%) under a base pressure of 3×10^{-5} Torr.

2.2. Macroscopic and microscopic morphology characterizations

Surface and cross-sectional morphologies of the coated aluminium alloy were observed by SEM (Quanta 250) and the corrosion depths were monitored via a laser confocal microscope (Keyence VK-X250) with a motorised z-axis stage to obtain precise morphological parameters such as the number of pits and pit depths. The phase structure of TiN and CrN films were analysed using X-ray diffraction (XRD, Bruker D8) with a Cu-K radiation.

2.3. Electrochemical measurements

Electrochemical measurements, including corrosion potential and potentiodynamic polarization, were performed using a Princeton VersaStudio 3F electrochemical workstation in a conventional 3-electrode cell: a platinum plate and a saturated calomel electrode (SCE) served as the counter and reference electrodes, respectively. A 3.5 wt. % NaCl solution, with a pH of approximately 6.0 was prepared. Potentiodynamic polarizations were initiated from a potential 10 mV lower than the corrosion potential to a positive direction, at a scanning rate of 0.1667 mV/s. All reported potentials in this work were relative to the SCE and electrochemical tests were conducted at room temperature (25 ± 1 °C).

2.4. Salt spray test

Salt spray tests were conducted according to the GB/T 10125—1997 standard. The aluminium alloys were subjected to ultrasonic cleaning in alcohol for 3 min and dried with a hot air flow. The salt spray test temperature was set as 35 °C, and the NaCl solution concentration was around (50 ± 5) g/L. The salt spray test cycles were 1, 3 and 7 d, respectively. After the salt spray test, the corrosion products were characterised through detailed morphology analyses performed using laser confocal microscopy and SEM.

3. RESULTS AND DISCUSSION

3.1 Surface morphology and composition

The cross-sectional and surface morphology of the TiN and ZrN coatings, and the related EDS results are shown in Figure 1 and we can see that the thickness of the coatings are uniform and the sizes of the TiN particles are a little larger than the CrN particles, and the element content on the top surface was all nitrides.

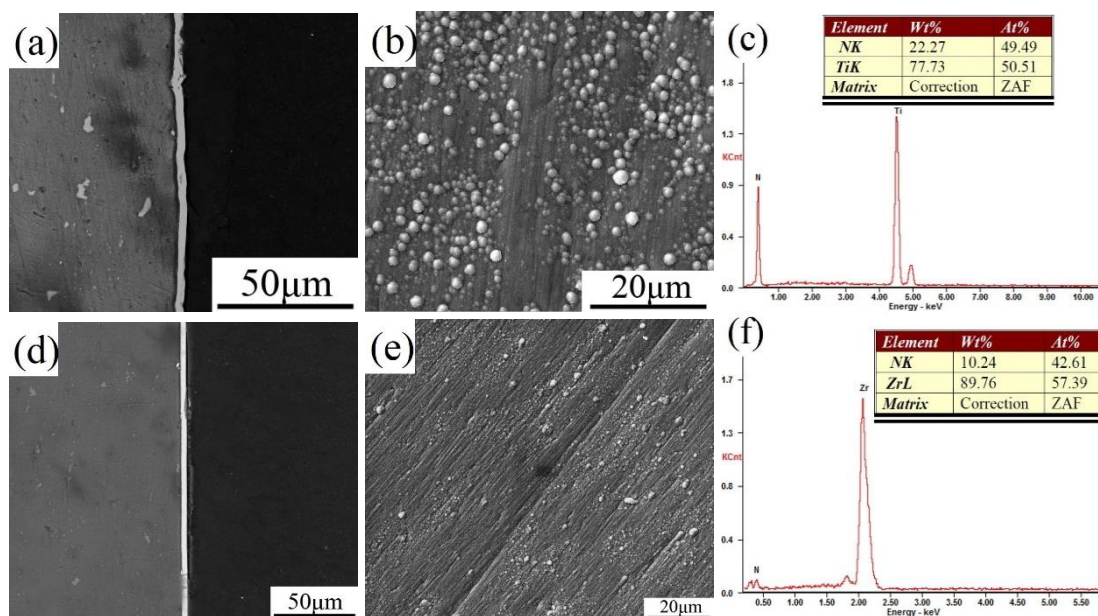


Figure 1. The cross-sectional morphology, surface morphology and the related EDS results: (a)(b)(c) TiN coating and (d)(e)(f) ZrN coating.

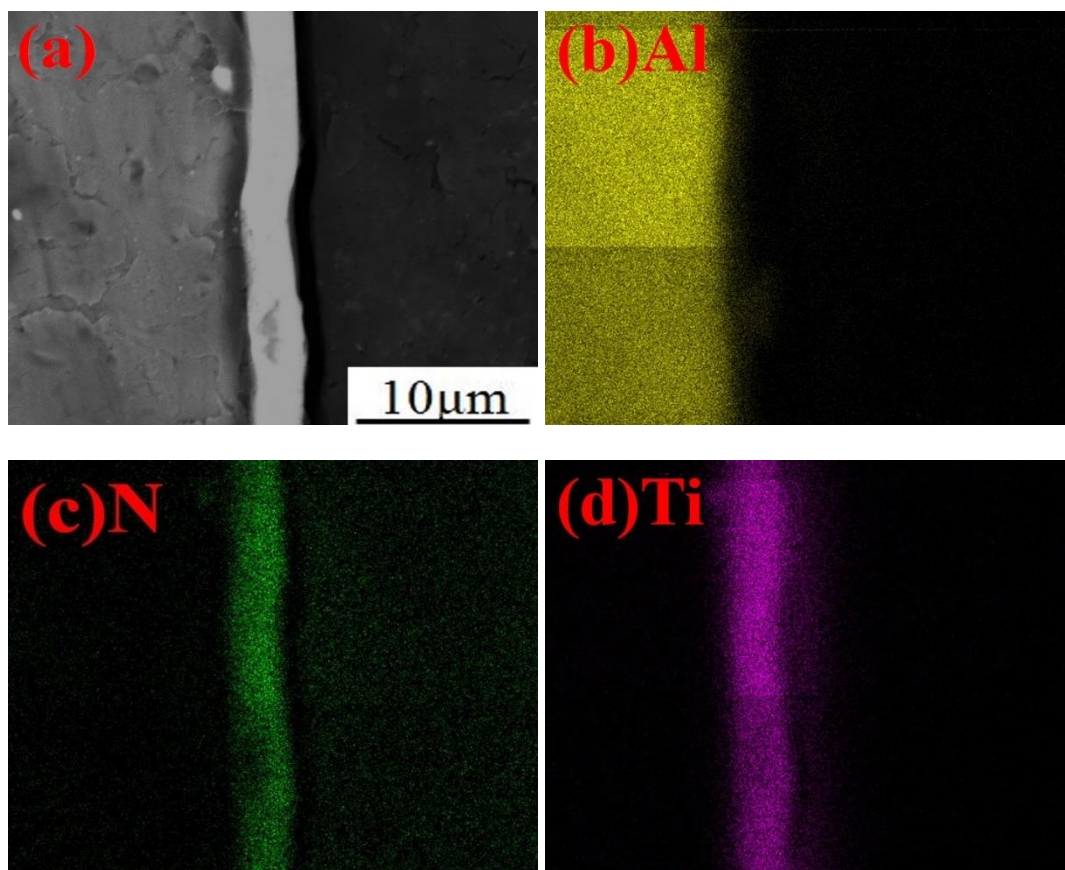


Figure 2. The cross-sectional morphology and the related EDS mapping results: (b) Al, (c) N and (d) Ti.

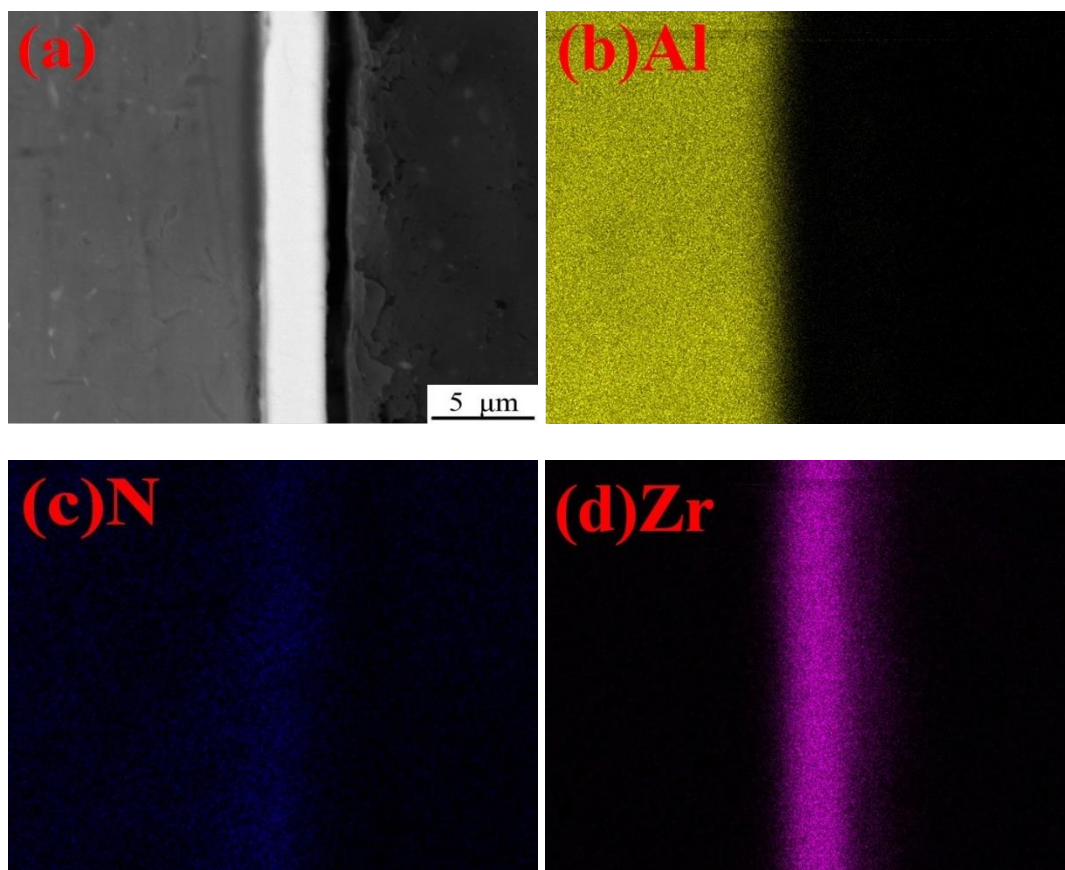


Figure 3. The cross-sectional morphology and the related EDS mapping results: (b) Al, (c) N and (e) Zr.

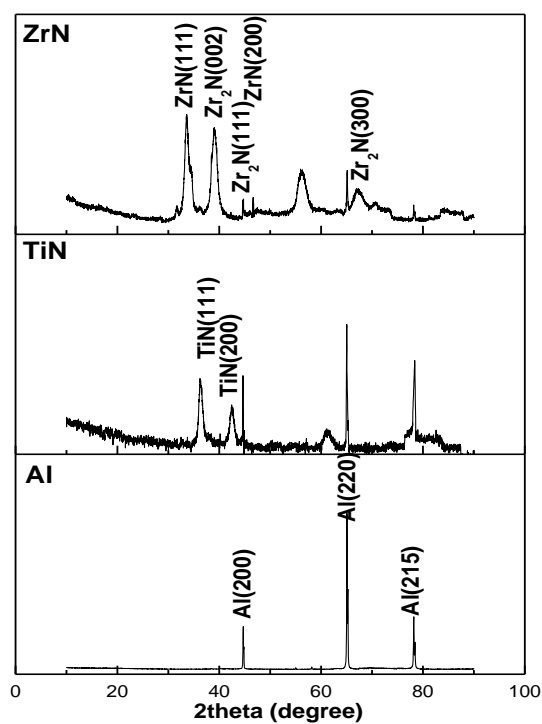


Figure 4. XRD patterns of the aluminum alloy, TiN and CrN coatings deposited on aluminum alloy.

To further confirm the element distribution, the EDS mapping results are shown in Figures 2 and 3, respectively. The thickness of these two coatings was the same (all around 2 μm) and the elements were distributed uniformly, indicating that a good coating layer was prepared.

Figure 4 shows the XRD patterns of TiN and CrN coatings deposited on the aluminium alloy. We can see there are still the strong signals of the aluminium alloy for the TiN coating that should be attributed to the defects widely existing in the coating so that it could not block the X-rays completely. However, the patterns were considerably better for the ZrN coating; the main phase for the CrN coating was fcc (PDF 65-2899) with a crystal orientation of the (200) plane, and is consistent with the columnar growth model in the magnetron sputtering method [26, 27]. The sharp diffraction peaks suggest that the crystallinity was very high and several other diffraction peaks were also observed by using XRD [28-30].

3.2 Electrochemical results

Potentiodynamic polarization curves of the bare aluminium alloy, TiN coating and ZrN coating in 3.5 wt. % NaCl solution are shown in Figure 5. The cathodic polarization can destroy the coating on the substrate to some extent, so the potentiodynamic polarizations were initiated from a potential a little lower than the open-circuit potential. We can see that the shape of polarization curves for the coated aluminium alloy is similar to that of the bare aluminium alloy, but with a lower corrosion current density for a same potential. Indeed, the corrosion potentials of both coatings are close to that of the aluminium alloy. The potential of CrN coated aluminium alloy is slightly less negative because of the formation of the chromium oxide layer during immersion testing. The decrease in corrosion current density is more noticeable in the TiN coated aluminium alloy than in the uncoated aluminium alloy as listed in Table 1 and it is still more noticeable for the CrN coated aluminium alloy, and the good overall anti-corrosion property of CrN/aluminium alloy specimens can be confirmed. The Tafel slopes of the anodic polarization curves (β_a) for the coated aluminium alloy are all higher than that of the bare aluminium alloy (around 5 times), which indicates a good protectiveness against corrosion for these two coatings in the short term [31]. To evaluate the durability during the long-term service, the salt spray tests are conducted accordingly.

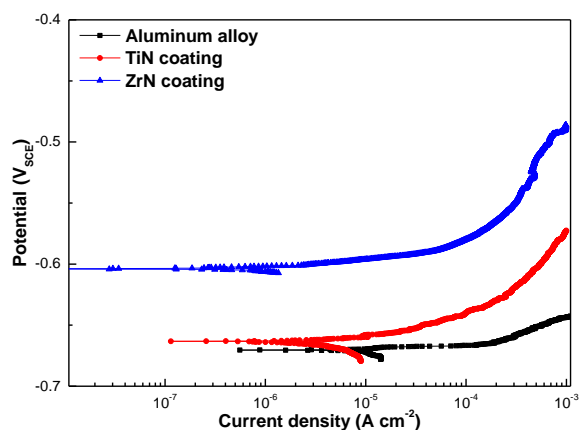


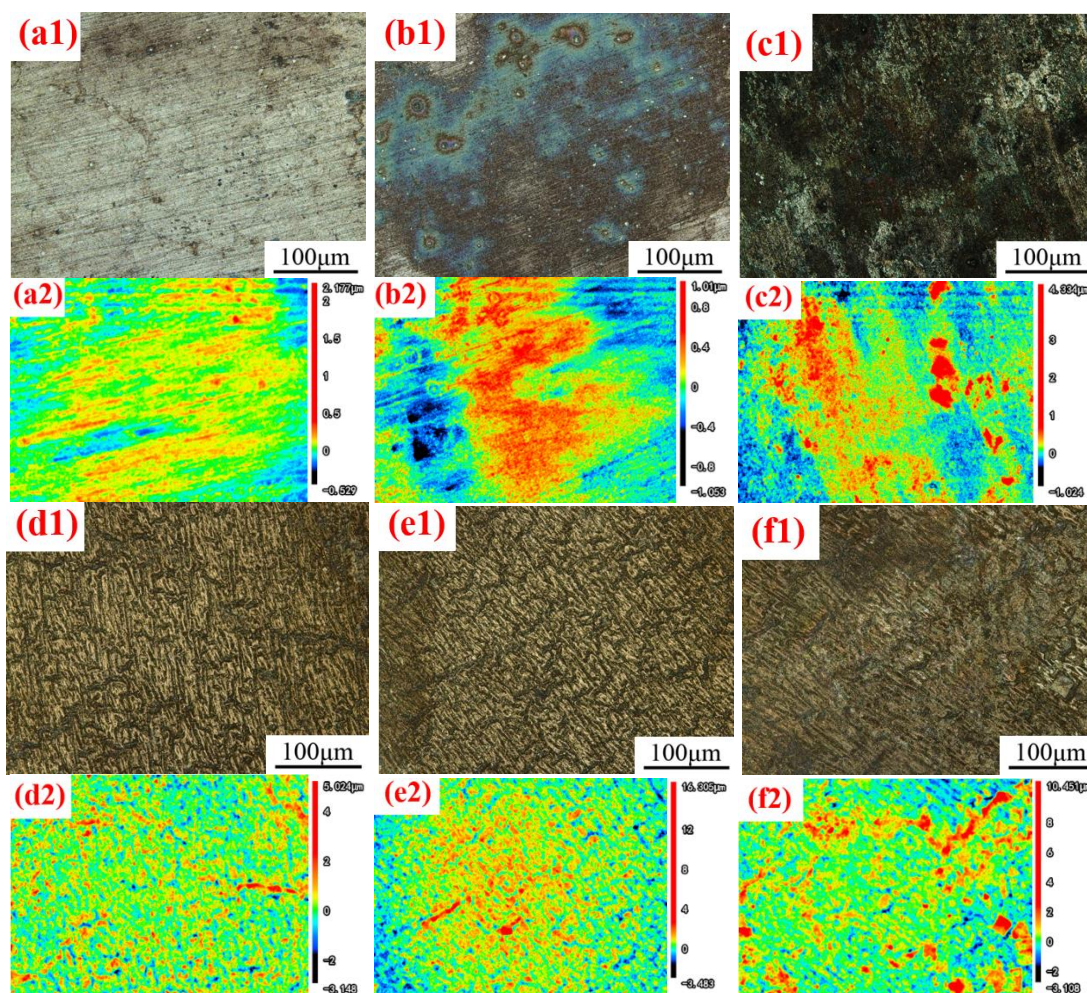
Figure 5. Potentiodynamic polarization curves of the bare aluminium alloy, TiN coating and ZrN coating in 3.5 wt. % NaCl solution. Scanning rate = 0.1667 mV/s.

Table 1. The electrochemical parameters obtained from the potentiodynamic polarization curves.

| | E_{corr} (VSCE) | I_{corr} ($\mu\text{A cm}^{-2}$) |
|----------------|--------------------|--------------------------------------|
| Aluminum alloy | -0.672 ± 0.012 | 13.1 ± 1.2 |
| TiN coating | -0.664 ± 0.008 | 4.8 ± 0.7 |
| ZrN coating | -0.605 ± 0.024 | 1.5 ± 0.3 |

3.3 Salt spray test

Salt spray test is a common method to evaluate the corrosion resistance of materials and Figure 6 presents the typical corrosion morphology and the 3-D morphology of the exposed plates after salt spray tests for 1, 3 and 7 days, respectively. We can see that the colour of the aluminium alloy became dark after long-term exposure, and the corrosion products accumulated on the top of the surface, and localised corrosion characteristics were observed obviously. For the TiN coating, there were grooves on the surface, and grey and white flocculated corrosion products could be seen in the grooves as shown in Figure 6 (f1). This should be attributed to the cracks formed during the magnetron sputtering process and for the ZrN coating, the surface did not change considerably except for a little salt deposition.



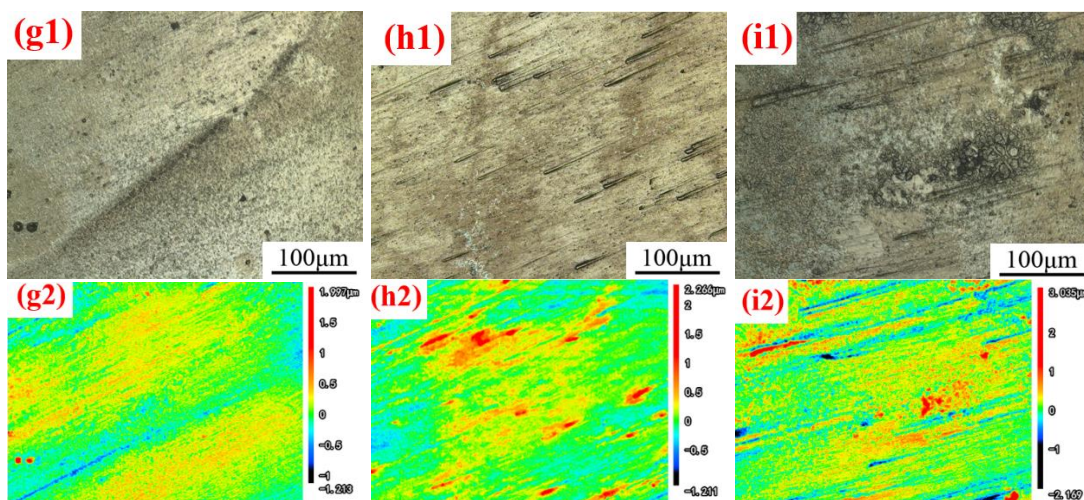
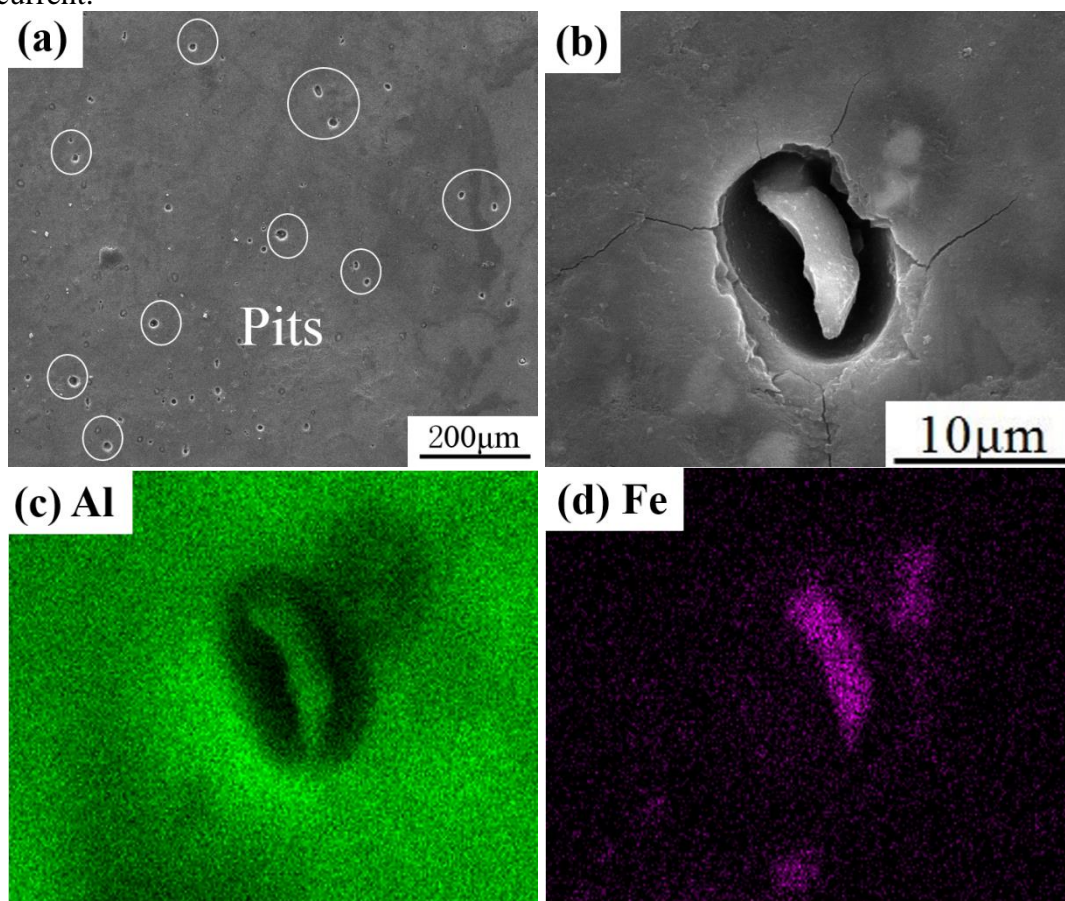


Figure 6. Typical pitting depth and 3-D morphology of the exposed plates after salt spray test: (a₁)(a₂)(b₁)(b₂)(c₁)(c₂) Cu, (d₁)(d₂)(e₁)(e₂)(f₁)(f₂) TiN coating and (g₁)(g₂)(h₁)(h₂)(i₁)(i₂) ZrN coating for 1, 3 and 7 days, respectively.

To further compare the corrosion morphology, the plates were observed via SEM after the salt spray test for 7 days and the results are displayed in Figures 7–9. We can see several pits in aluminium alloys in the chloride environment as shown in Figure 7 (a). Noble precipitates with high electrochemical activity, such as Al₂Cu, Al₇Cu₂Fe [32], widely existed in the aluminium alloy and such intermetallics are possibly associated to peripheral pitting as shown in Figure 8 (a), with the ability to sustain a large cathodic current.



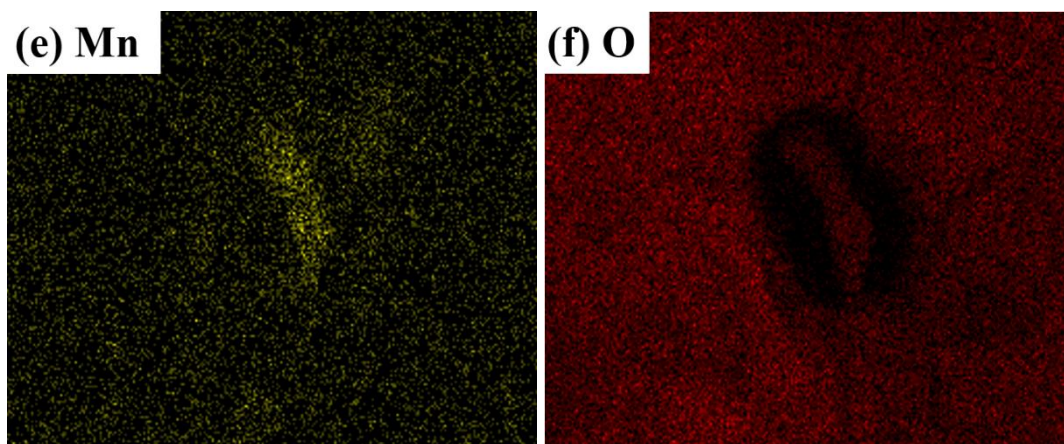
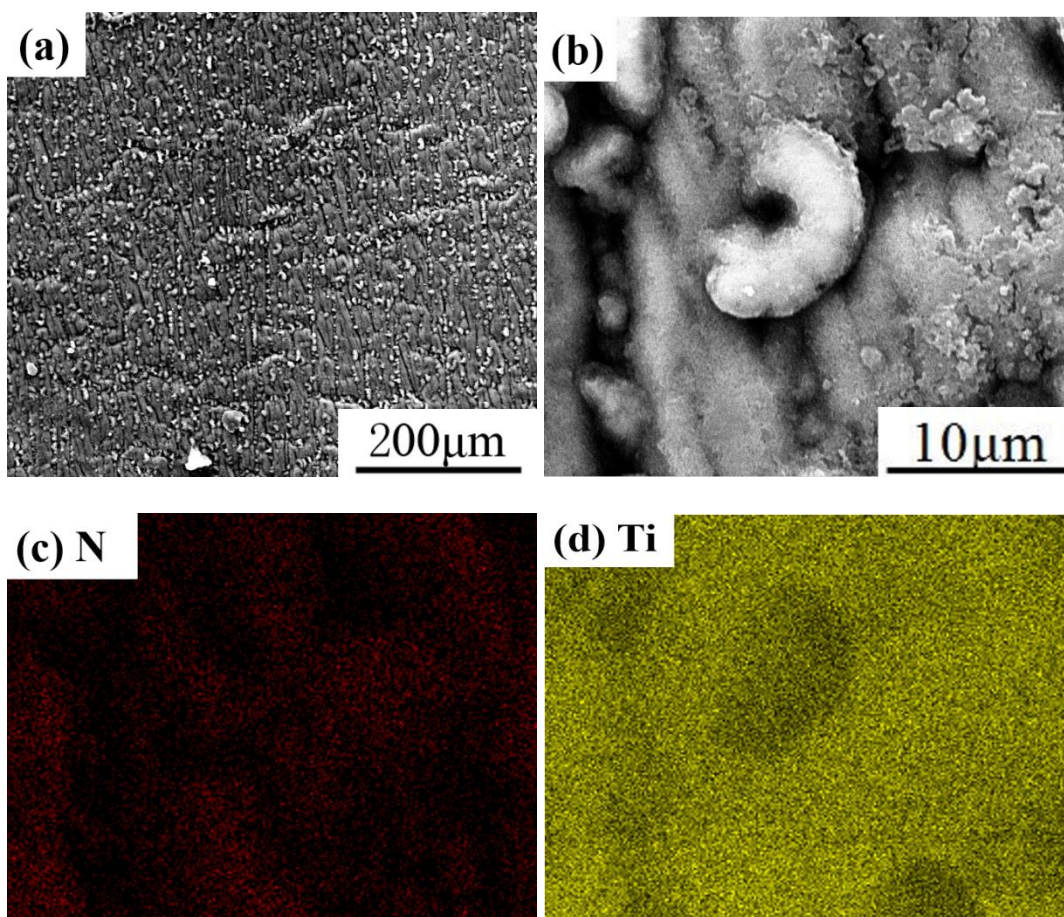


Figure 7. (a) (b) Surface morphology of the pitting morphology and the corresponding elemental mapping images (c) Al, (d) Fe, (e) Mn and (f) O.



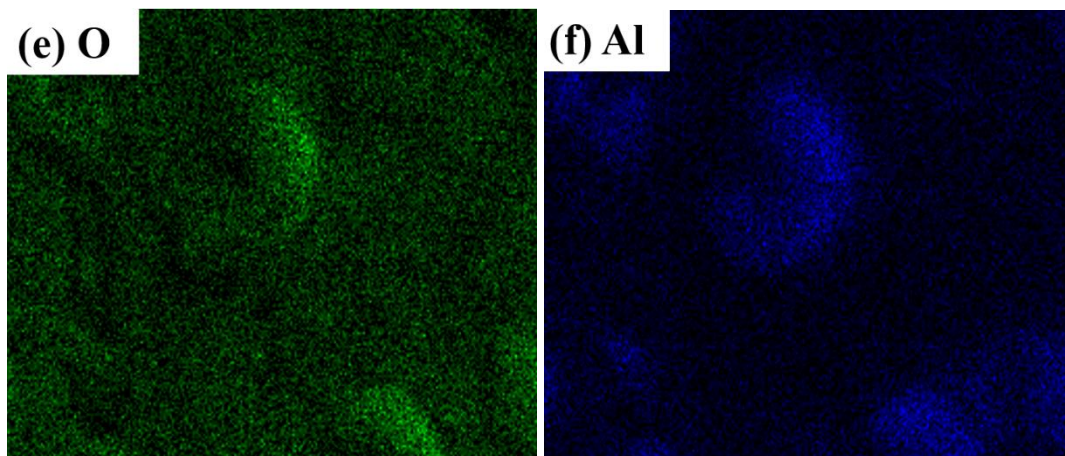
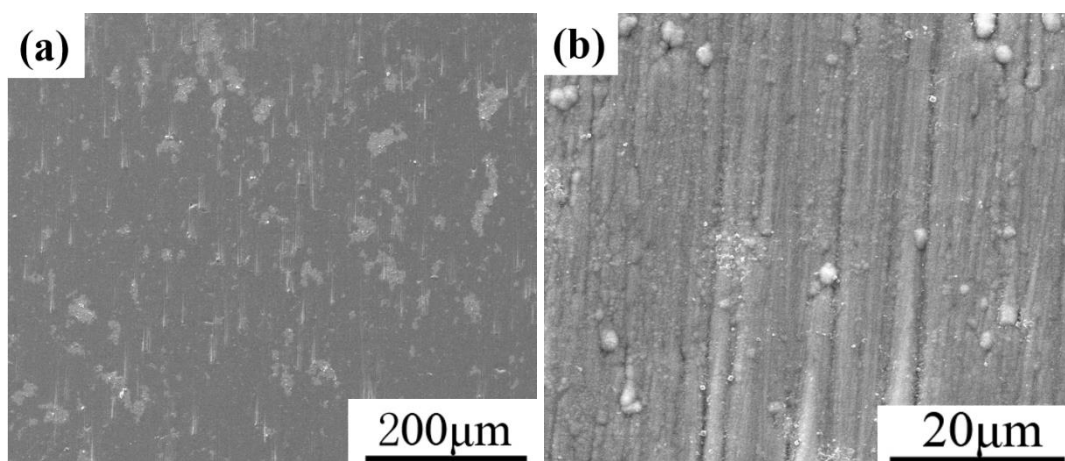


Figure 8. (a)(b) Surface morphology of the TiN coating and the corresponding elemental mapping images (c) N, (d) Ti, (e) O and (e) Al.

The EDS results confirmed that the intermetallics in Figure 7(b) were α -Al (Fe, Mn) particles [33], which have a higher self-corrosion potential in sodium chloride solution than the aluminium matrix [34], and the surrounding sites preferred to dissolve and thus pitting occurred, and this was why surface treatments were widely adopted on the aluminium alloy.

Figure 8 shows the surface morphology of the TiN coating on the aluminium alloy after the salt spray test for 7 days and we can see that there were some corrosion clusters existing in the grooves of the coating that are attributed to the corrosion products of the aluminium substrate. This inferior corrosion performance is not a result of the intrinsic corrosion behaviour of the nitride coating itself, but rather results from the small structural defects during the magnetron sputtering process, which act as channels for the aggressive ions to permeate into and attack the substrate. However, this did not occur on the ZrN coating, and the coating was still intact and the elements of N and Zr were distributed uniformly, indicating a desirable corrosion resistance after long-term service.



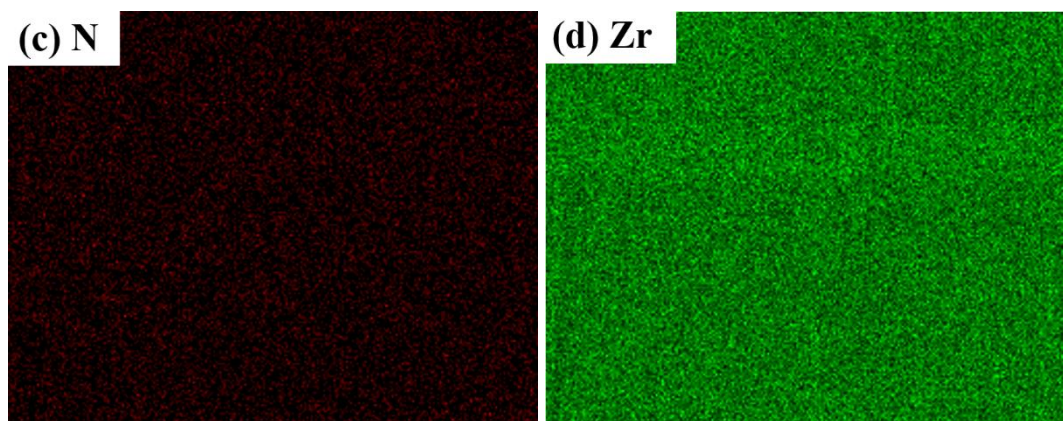


Figure 9. (a)(b) Surface morphology of the ZrN coating and the corresponding elemental mapping images (c) N and (d) Zr.

4. CONCLUSIONS

This study compared the corrosion resistance of CrN and TiN coatings on aluminium alloy with the same thickness, and electrochemical techniques such as potentiodynamic measurement, and salt spray tests were conducted. The findings led to the following conclusions:

1. CrN coating exhibited an excellent corrosion resistance on aluminium alloy when compared to TiN coating with the same thickness.
2. The inferior corrosion performance of TiN coating is a result of small structural defects during the magnetron sputtering process, e.g. pinholes and cracks, which act as channels for the subsequent corrosion of the substrate.

ACKNOWLEDGEMENTS

This work was supported by the National Key Research and Development Program of China (No. 2017YFB 0702300), National Natural Science Foundation of China (No. 51671029) and Fundamental Research Funds for the Central Universities (No. FRF-TP-17-002B).

References

1. C.B. Zheng, B.H. Yan, K. Zhang and G. Yi, *Int. J. Min. Met. Mater.* 22 (2015) 729-737.
2. B.R.G and N. Birbilis, *J. Electrochem. Soc.* 152 (2005) 467.
3. B. Hou, X. Li, X. Ma, C. Du, D. Zhang, M. Zheng, W. Xu, D. Lu and F. Ma, *npj Mater. Degrad.* 1 (2017) 1.
4. X. Li, D. Zhang, Z. Liu, Z. Li, C. Du and C. Dong, *Nature* 527 (2015) 441-442.
5. C.D. Taylor, P. Lu, J. Saal, G.S. Frankel and J.R. Scully, *npj Mater. Degrad.* 2 (2018) 1.
6. S. Gin, P. Dillmann and N. Birbilis, *npj Mater. Degrad.* 1 (2017) 1.
7. D. Kong, C. Dong, Z. Zheng, F. Mao, A. Xu, X. Ni, C. Man, J. Yao, K. Xiao and X. Li, *Appl. Surf. Sci.* 440 (2018) 245.
8. H. Luo, C.F. Dong, X.G. Li and K. Xiao, *Electrochim. Acta* 64 (2012) 211.
9. Z.C. Feng, X.Q. Cheng, C.F. Dong, L. Xu and X.G. Li, *Corros. Sci.* 52 (2010) 3646.
10. D. Kong, X. Ni, C. Dong, L. Zhang, C. Man, J. Yao, K. Xiao and X. Li, *Electrochim. Acta* 276 (2018) 293.

11. D.C. Kong, A.N. Xu, C.F. Dong, F.X. Mao, K. Xiao, X.G. Li and D.D. Macdonald, *Corros. Sci.* 116 (2017) 34.
12. C.F. Dong, X.G. Li, Z.Y. Liu and Y.R. Zhang, *J. Alloy Compd.* 484 (2009) 966.
13. D. Kong, X. Ni, C. Dong, X. Lei, L. Zhang, C. Man, J. Yao, X. Cheng and X. Li, *Mater. Design* 152 (2018) 88.
14. R. Akid, M. Gobara and H. Wang, *Electrochim. Acta* 56 (2011) 2483.
15. M. Niknahad, S. Moradian and S.M. Mirabedini, *Corros. Sci.* 52 (2010) 1948.
16. A. Persson, J. Bergstrom, C. Burman and S. Hogmark, *Surf. Coat. Tech.* 146 (2001) 42.
17. B. Yin, L. Fang, A.Q. Tang, Q.L. Huang, J. Hu, J.H. Mao, G. Bai and H. Bai, *Appl. Surf. Sci.* 258 (2011) 580.
18. Z. Feng, Y. Liu, G.E. Thompson and P. Skeldon, *Electrochim. Acta* 55 (2010) 3518.
19. C.F. Dong, Z.Y. Liu, X.G. Li and Y.F. Cheng, *Int. J. Hydrogen Energ.* 34 (2009) 9879.
20. H. Luo, C.F. Dong, K. Xiao and X.G. Li, *Appl. Surf. Sci.* 258 (2011) 631.
21. C.F. Dong, A.Q. Fu, X.G. Li and Y.F. Cheng, *Electrochim. Acta* 54 (2008) 628.
22. B. Subramanian and M. Jayachandran, *Mater. Lett.* 62 (2008) 1727.
23. M. Balzer, *Thin Solid Films* 581 (2015) 99.
24. M. Flores, L. Huerta, R. Escamilla, E. Andrade and S. Muhl, *Appl. Surf. Sci.* 253 (2007) 7192.
25. P.J. Kelly and R.D. Arnell, *Vacuum* 56 (2000) 159.
26. Y. Shi, S. Long, L. Fang, F. Pan and H. Liao, *Appl. Surf. Sci.* 255 (2009) 6515.
27. S. Tan, X. Zhang, X. Wu, F. Fang and J. Jiang, *Appl. Surf. Sci.* 257 (2011) 5595.
28. Y. Li, L. Qu and F. Wang, *Corros. Sci.* 45 (2003) 1367.
29. J. Creus, H. Idrissi, H. Mazille, F. Sanchette and P. Jacquot, *Surf. Eng.* 14 (2013) 432.
30. S. Gao, C. Dong, H. Luo, K. Xiao, X. Pan and X. Li, *Electrochim. Acta* 114 (2013) 233.
31. D. Kong, C. Dong, X. Ni, C. Man, K. Xiao and X. Li, *Appl. Surf. Sci.* 455 (2018) 543.
32. S. Li, H. Dong, L. Shi, P. Li and F. Ye, *Corros. Sci.* 123 (2017) 243.
33. J. Kang, R.D. Fu, G.H. Luan, C.L. Dong and M. He, *Corros. Sci.* 52 (2010) 620.
34. B.M. Aballe and F. J. Botana, *Corros. Sci.* 43 (2001) 1657.